We are IntechOpen,
the world's leading publisher of
Open Access books
Built by scientists, for scientists

6,900
Open access books available

186,000
International authors and editors

200M
Downloads

Our authors are among the

154
Countries delivered to

TOP 1%
most cited scientists

12.2%
Contributors from top 500 universities

WEB OF SCIENCE™

Selection of our books indexed in the Book Citation Index
in Web of Science™ Core Collection (BKCI)

Interested in publishing with us?
Contact book.department@intechopen.com

Numbers displayed above are based on latest data collected.
For more information visit www.intechopen.com

3

Rectifying Acoustic Waves

Yukihiro Tanaka, Takahiro Murai, and Norihiko Nishiguchi
Department of Applied Physics, Hokkaido University
Sapporo 060-8628, Hokkaido,
Japan

1. Introduction

Diodes play an essential and important role in controlling current flow in the electric circuits. The rectification mechanisms utilize thermo electrons in vacuum tubes and the difference in energy band structures between $p – n$ junctions of semiconductors. Ever since the advent of nanotechnology, efforts were made to realize a nano diode, and rectification of current is achieved by using geometric effects on electron scattering by asymmetric scatterers.(Song et al., 1998; Fleischmann & Geisel, 2002; Linke et al., 1998). In contrast, the rectification mechanism of acoustic waves is not established, and then rectification mechanisms of acoustic waves attract much attention from both theoretical (Liang et al., 2009) and experimental viewpoints (Chang et al., 2006).

Recent theoretical work proposed a rectification mechanism of acoustic waves utilizing mode conversion of acoustic waves owing to elastic anharmonicity in the constituent materials (Liang et al., 2009), and then the efficiency of rectification of the proposed model depends on the amplitude of acoustic waves. In addition, there is difficulty in finding suitable materials for fabricating the system.

We have proposed a rectification mechanism for acoustic waves (Krishnan et al., 2007;Shirota et al., 2007) based on geometric effects on scattering of acoustic waves by asymmetric scatterers, and have confirmed, with numerical simulations, the rectification effects of acoustic waves for bulk acoustic waves (Krishnan et al., 2007; Shirota et al., 2007), and Rayleigh waves in the surface (Tanaka et al., n.d.). In this chapter, we review the rectification mechanism, and illustrate the capability of rectification for bulk acoustic waves, and Rayleigh waves, respectively. Surface acoustic waves (SAWs) are exploited in a variety of devices, and then the proposed rectification mechanism is expected to provide novel functions to the acoustic wave devices.

The chapter is organized as follows; we introduce a model of rectifier for acoustic waves, and provide the methodology in §2. The numerical results for bulk transverse and longitudinal waves and Rayleigh waves in the surface are given in §3. A summary and future prospects are given in §4.

2. Model and methodology

The acoustic wave rectifier to be discussed consists of an elastically isotropic material containing a one-dimensional array of isosceles-triangular holes with summit angle α in the y direction, whose axis is in the z direction as shown in Fig. 1(a). The distance between the
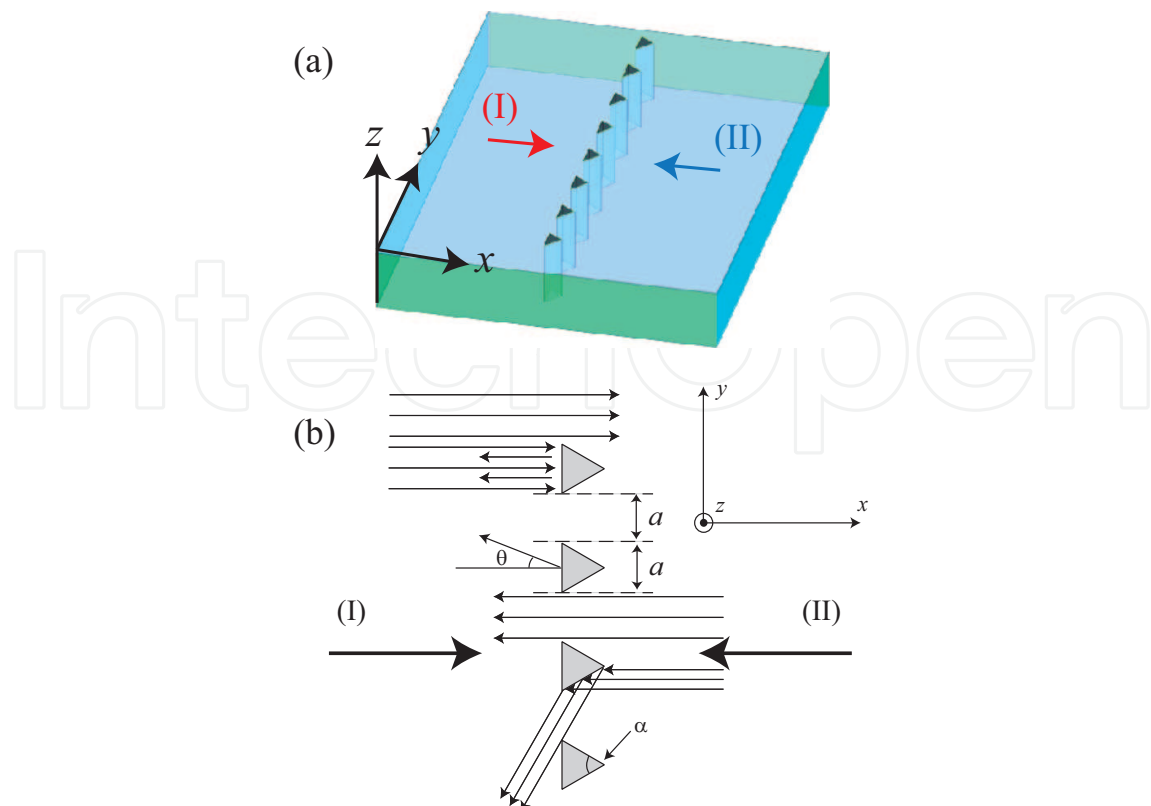
Fig. 1. (a) Schematic view of our model that shows the rectification effect for acoustic waves. (b) z–polarized transverse acoustic wave reflection from isosceles-triangular holes drilled in an elastically isotropic material. The triangles are separated by the same distance as the base, and are aligned in the y direction. The thick arrows indicate the directions (I) and (II) of incident waves. The thin arrows show reflection and transmission of waves in the very short wavelength limit, where the diffraction is ignored.

neighboring triangles is the same as the base length a of the triangles (thus the periodicity in the y direction is $D = 2a$). The holes are left empty in order to get strong reflection of acoustic waves.

Rectification for acoustic waves with very short wavelength in this system is apparent. Considering case (I) that acoustic rays propagate from the left region toward a matrix with equilateral-triangular holes ($\alpha = \pi/3$) of periodically aligned in the y direction as shown in Fig. 1(b), one half of them are scattered backward, and the rest passes between the scatterers. The resultant transmission rate becomes 0.5. On the other hand, the transmission rate becomes 1 for case (II) where the rays impinge on the summits of the triangular voids from the right region, since the rays reflected from the surface are transmitted to the left region through the passes between the holes. Thus the acoustic waves are rectified in the very short wavelength limit.

The prediction by the ray-acoustics cannot be immediately applied to the wave propagation at finite wavelength because of decay in the geometric effects and of interference effects. The waves peculiar to the geometry of scatterers decay near the scatterers and only the azimuthally symmetric waves propagate in the asymptotic field as a cylindrical wave in a two-dimensional (2D) system or a spherical wave in a 3D one. Thus the rectification seems impossible for finite wavelength, however, the present system works as a rectifier for acoustic waves as shown below.

Here we consider acoustic waves propagating through an array of triangular holes drilled in an isotropic material. In this case the equations of motion governing the displacement vectors **u**(**r**, *t*) are given by

$$\rho(\mathbf{x})\ddot{u}_i(\mathbf{r},t) = \partial_j \sigma_{ij}(\mathbf{r},t) \quad (i = 1,2,3) \tag{1}$$

$$\sigma_{ij}(\mathbf{r},t) = c_{ijmn}(\mathbf{x})\partial_n u_m(\mathbf{r},t) \tag{2}$$

where **r** = (**x**, *z*) = (*x*,*y*, *z*) and the summation convention over repeated indices is assumed in Eqs. (1) and (2). $\rho(\mathbf{x})$ and $c_{ijmn}(\mathbf{x})$ are the position-dependent mass density and elastic stiffness tensor of the system, and $\sigma_{ij}(\mathbf{r}, t)$ is the stress tensor. Furthermore, we need to impose proper boundary conditions for SAWs. SAWs should satisfy the stress-free boundary condition at the surface $z = 0$, or

$$\sigma_{i3}\big|_{z=0} = c_{i3mn}\partial_n u_m\big|_{z=0} = 0 \quad (i = 1,2,3). \tag{3}$$

Solving the equations with finite-difference time-domain (FDTD) method numerically, we can obtain the time evolutions of displacement vectors **u**(**r**, *t*) and stress tensors $\sigma_{ij}(\mathbf{r}, t)$ at each point in the system. To calculate the transmission rate through the periodic array of triangle holes, we define the acoustic Poynting vector $J_i(\mathbf{r}, t) = -\dot{u}_j(\mathbf{r}, t)\sigma_{ji}(\mathbf{r}, t)$ from the continuity of energy flow. In terms of the Fourier components of the displacement $\hat{\mathbf{u}}(\mathbf{r},\omega)$ and the stress tensor $\hat{\sigma}_{ij}(\mathbf{r},\omega)$, the energy flow at frequency ω in the x direction at the position x is expressed by

$$\hat{J}_x(x,\omega) = -4\pi \int \text{Im}\left[\omega \hat{u}_j(\mathbf{r},\omega)\hat{\sigma}_{jx}^*(\mathbf{r},\omega)\right]dydz. \tag{4}$$

Hence we can determine the transmission rate $T(\omega)$ by the ratio of the element of the acoustic Poynting vector in the x direction $\hat{J}_x(x_D,\omega)$ to that in the absence of scatterers $\hat{J}_x^0(x_D,\omega)$, which is given by

$$T(\omega) = \frac{\hat{J}_x(x_D,\omega)}{\hat{J}_x^0(x_D,\omega)}, \tag{5}$$

where x_D is the detecting position which is on the right side of the scatterers for case (I) and on the left side of the scatterers for case (II). We introduce an efficiency $\eta(\omega)$ to quantify rectification by

$$\eta(\omega) = \left|\frac{T_\text{I}(\omega) - T_\text{II}(\omega)}{T_\text{I}(\omega) + T_\text{II}(\omega)}\right| \tag{6}$$

where T_I and T_II are the transmission rates for cases (I) and (II), respectively.

3. Numerical results

3.1 Bulk acoustic waves
In the section we illustrate the rectifying effects of bulk acoustic waves propagating in the *x*-direction. Because of the homogeneity in the *z* direction, the governing equations (1) and (2) are decoupled into two independent sets; one is expressed by

$$\rho(\mathbf{x})\frac{\partial^2 u_z(\mathbf{x},t)}{\partial t^2} = \frac{\partial \sigma_{zx}(\mathbf{x},t)}{\partial x} + \frac{\partial \sigma_{zy}(\mathbf{x},t)}{\partial y},$$

$$\sigma_{zx}(\mathbf{x},t) = C_{44}(\mathbf{x})\frac{\partial u_z(\mathbf{x},t)}{\partial x},$$

$$\sigma_{zy}(\mathbf{x},t) = C_{44}(\mathbf{x})\frac{\partial u_z(\mathbf{x},t)}{\partial y},$$

where the acoustic wave is z-polarized transverse wave, referred to as *single mode*. Another is the acoustic waves termed *mixed modes* with polarization in the $x - y$ plane, which obey

$$\rho(\mathbf{x})\frac{\partial^2 u_x(\mathbf{x},t)}{\partial t^2} = \frac{\partial \sigma_{xx}(\mathbf{x},t)}{\partial x} + \frac{\partial \sigma_{xy}(\mathbf{x},t)}{\partial y},$$

$$\rho(\mathbf{x})\frac{\partial^2 u_y(\mathbf{x},t)}{\partial t^2} = \frac{\partial \sigma_{xy}(\mathbf{x},t)}{\partial x} + \frac{\partial \sigma_{yy}(\mathbf{x},t)}{\partial y},$$

$$\sigma_{xx}(\mathbf{x},t) = C_{11}(\mathbf{x})\frac{\partial u_x(\mathbf{x},t)}{\partial x} + C_{12}(\mathbf{x})\frac{\partial u_y(\mathbf{x},t)}{\partial y},$$

$$\sigma_{yy}(\mathbf{x},t) = C_{12}(\mathbf{x})\frac{\partial u_x(\mathbf{x},t)}{\partial x} + C_{11}(\mathbf{x})\frac{\partial u_y(\mathbf{x},t)}{\partial y},$$

$$\sigma_{xy}(\mathbf{x},t) = C_{44}(\mathbf{x})\left(\frac{\partial u_x(\mathbf{x},t)}{\partial y} + \frac{\partial u_y(\mathbf{x},t)}{\partial x}\right),$$

The mixed modes consist of longitudinal and transverse waves due to the scattering by the triangular voids since the mode conversion between the longitudinal and transverse waves takes place for scattering.

3.1.1 Single mode

Figure 2 shows the transmission rates versus frequency in the case of equilateral-triangular holes ($\alpha = \pi/3$) and isosceles-triangular holes ($\alpha = 2\pi/9$) for two opposite incident directions (I) and (II). For both types of triangular holes, there is not noticeable difference in the transmission rates between the two incident directions at low frequency; $\omega a/v_t < \pi$. On the other hand, we find remarkable dependence in the transmission rates on the incident directions at $\omega a/v_t > \pi$. Above the threshold frequency $\omega_{\mathrm{th}} a/v_t = \pi$, the transmission rate for (I) is approximately $T = 0.5$ that is the same as the magnitude predicted from the ray-acoustics, showing small dips in magnitude at the multiples of the threshold frequency. The transmission rate for (II) is larger than that for (I), and also shows periodic dips in magnitude with the same period as (I). The obvious difference in the transmission rates above the threshold frequency between (I) and (II) indicates that the rectification occurs at the wavelength comparable to the dimension of scatterers, i. e. $a/\lambda > 1/2$ due to the linear dispersion relation $\omega = kv_t = 2\pi v_t/\lambda$. Although the periodic dips, which appear when $\omega a/v_t = n\pi$ ($n = 1, 2, 3, \ldots$), are common to both the equilateral- and isosceles-triangular holes, the latter system has advantageous properties for rectification of acoustic waves; the transmission rates for (II) of $\alpha = 2\pi/9$ are larger than those for $\alpha = \pi/3$. This indicates that the rectification is enhanced with decreasing α.
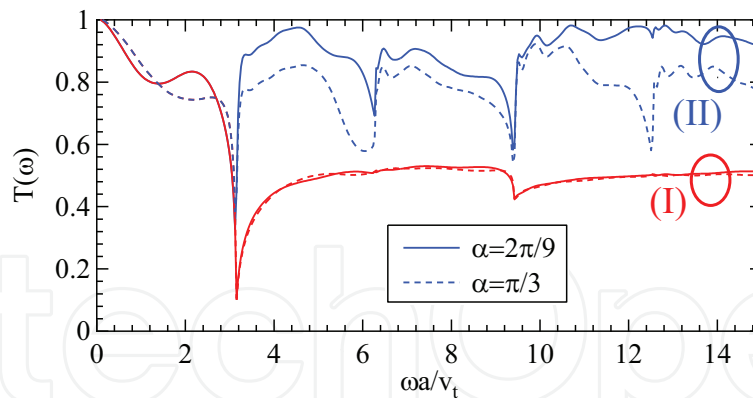
Fig. 2. Transmission rate versus frequency. The dashed and solid lines indicate the transmission rate for $\alpha = \pi/3$ and $2\pi/9$, respectively. Each case of (I) and (II) is bundled with an ellipse.

Within the ray acoustics approximation, the transmission rate of (II) is expected to be 1 for $\alpha < \pi/3$ and 0.5 for $\alpha > \pi/2$, and varies as $T = (1/2) + \cos\alpha$ for $\pi/3 < \alpha < \pi/2$. On the other hand, the transmission rate of (I) becomes 0.5, independent of α. For finite wavelength, the transmission rate changes with α as shown in Fig. 2, showing a larger transmission rate at $\alpha = 2\pi/9$ than that at $\alpha = \pi/3$. From the results, we expect that the rectification effects decay with increasing α. To investigate the angle dependence, we examine the change in the transmission rates for variation of α. Generating a wave packet having a Gaussian spectral distribution of central frequency $\omega_C = (5\pi/2)(v_t/a)$ with $\Delta\omega = (\pi/2)(v_t/a)$, we evaluate the transmission rate for the wave packet, defining

$$T = \frac{\iint \int_{\omega_C-\Delta\omega}^{\omega_C+\Delta\omega} \hat{J}_x(x_D,\omega) d\omega dy dz}{\iint \int_{\omega_C-\Delta\omega}^{\omega_C+\Delta\omega} \hat{J}_x^0(x_D,\omega) d\omega dy dz}. \tag{7}$$

Figure 3 plots the transmission rates defined by Eq. (7) versus α. The difference in the transmission rates decreases with increasing α. However, the rectification effects survive for $\alpha > \pi/2$. We also find that the transmission for (I) is slightly larger than 0.5. We can regard these deviations from the predictions based on the ray acoustics as diffraction effects.

The threshold frequency for the rectification and the periodic change in the transmission rate originate from the interference effects. Because of the periodic structure in the y-direction, the wavenumber in the y direction is discretized in unit of $\frac{n\pi}{a}$, so that the dispersion relation of the acoustic waves becomes subband structure given by

$$\omega = v_t k = v_t \sqrt{k_x^2 + \left(\frac{n\pi}{a}\right)^2}, \tag{8}$$

where n is an integer. Figure 4 shows the dispersion relation of single mode for the summit angle $\alpha = \pi/3$ together with the corresponding transmission rate. When the incident waves with $k_y = 0$ are elastically scattered, the waves are transited to the waves with finite k_y. However, below the threshold frequency $\omega_{th}a/v_t$, there is no waves with finite k_y, so that the incident waves in the x-direction are scattered only forward or backward, even if the waves are scattered from the legs of triangles, resulting in the transmission rates independent of the incident-wave directions.
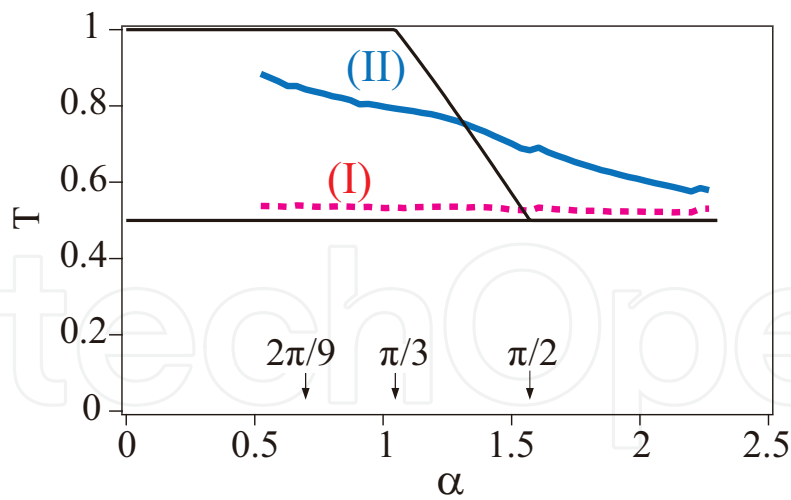
Fig. 3. Transmission rate defined by Eq. (7) versus the summit angle α. The thick dashed and solid lines indicate the transmission rate for cases (I) and (II), respectively. The thin solid lines indicate the transmission rates for (I) and (II) based on the ray acoustics.
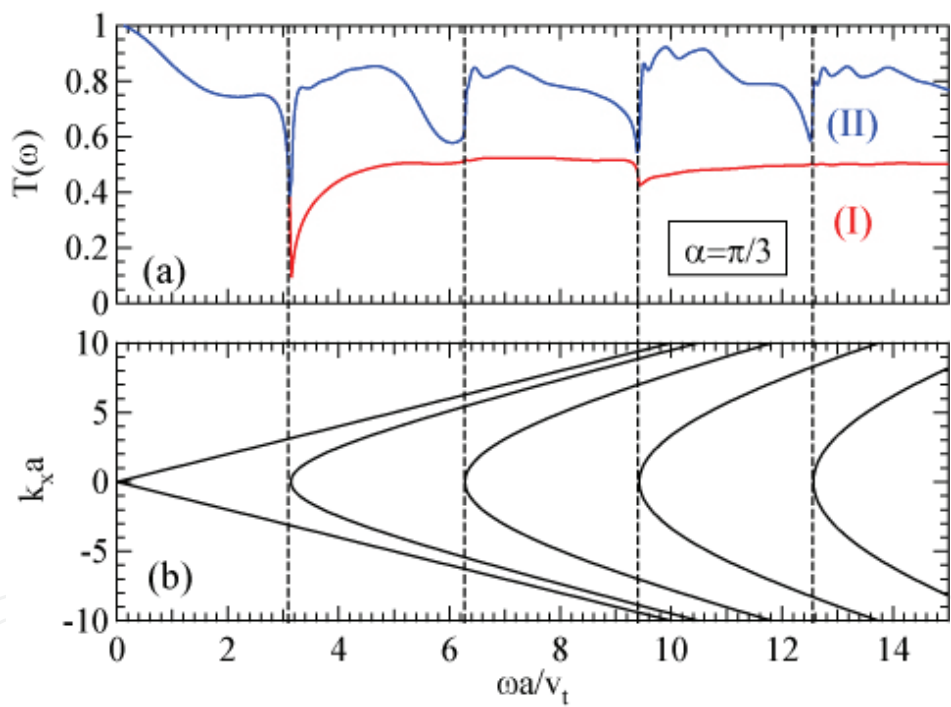

Fig. 4. (a) Transmission rate versus frequency for single modes through single-array of triangular holes with $\alpha = \pi/3$. The labels (I) and (II), designated by red and blue solid line, respectively, indicate the incident direction of acoustic waves. The vertical dashed lines indicate the positions of $n\pi v_t/a$, where $n = 1, 2, \ldots$ where v_t are the velocity of transverse waves. (b) Dispersion relation of single modes within the empty-lattice approximation.

Redirection of the incident waves for scattering occurs only in the frequency region above the threshold frequency. Since each dispersion relation of the waves with finite k_y becomes minimum at $k_x = 0$, the density of states diverges, resulting in remarkable scattering into the waves with finite k_y and $k_x = 0$ when the frequency matches the subband bottoms. The

geometry of the scatterers enhances or suppresses the redirection depending on the incident directions of the wave. Hence, the rectification occurs only above the threshold frequency and the dips in the transmission rates take place.

3.1.2 Mixed mode

The transmission rates versus frequency for mixed modes are shown in Fig. 5, when the longitudinal waves are transmitted. We assumed the matrix made of tungsten, whose the mass density ρ and the elastic stiffness tensors C_{11}, C_{44} are 19.317g cm^{-3} and 5.326×10^{12}dyn cm^{-2}, 1.631 × 10^{12}dyn cm^{-2}, respectively. The velocities of bulk longitudinal and transverse waves are v_l = 5.25 × 10^{5}cm s^{-1} and v_t = 2.906 × 10^{5}cm s^{-1}. (Kittel, 2004)

The red and blue solid lines indicate two different incident directions (I) and (II), respectively. The two transmission rates agree for $\omega a/v_t < \pi$, and we can see the difference between the transmissions for $\omega a/v_t > \pi$, although it is not as large as that for the single modes, manifesting rectification of the mixed modes. Unlike the single modes, we can see two kinds of periodic changes in transmission rates above $\omega a/v_t = \pi$, one is periodic modulation with period $\Delta \omega a/v_t = \pi$, indicated by the black dashed vertical lines, and another is periodic variations with period $\Delta \omega a/v_t = \pi \times v_l/v_t \sim 1.807\pi$, indicated by the green ones. In addition, some aperiodic dips in the transmission rate indicated by the arrows appear above $\omega a/v_t = \pi$. These dips shift when the shape of the triangular hole changes. Very interestingly there is no rectification in high frequency regions ($\omega a/v_t > 13$) because, for the waves impinging on the summit, the mode conversion from longitudinal waves to transverse ones is strongly caused and the scattered transverse waves return to the incident direction.

3.2 Surface acoustic waves

Figure 6(a) shows the frequency dependences of the transmission rates for SAWs with the incident-wave directions (I) and (II) which are denoted by red and blue solid lines, respectively. For numerical evaluation, the matrix is assumed to be polycrystalline silicon regarded as an isotropic medium, where the mass density ρ and the stiffness tensors C_{11}, C_{44} are 2.33g cm^{-3} and 1.884 × 10^{12}dyn cm^{-2}, 0.680 × 10^{12}dyn cm^{-2}, respectively. (Tamura, 1985) Then the velocities of bulk longitudinal and transverse waves are v_l = 8.99 × 10^{5}cm s^{-1} and v_t = 5.40 × 10^{5}cm s^{-1}, respectively. The equation for the velocity of a Rayleigh wave in an isotropic medium with a surface is given by

$$\xi^6 - 8\xi^4 + 8\xi^2\left(3 - 2\frac{v_t^2}{v_l^2}\right) - 16\left(1 - \frac{v_t^2}{v_l^2}\right) = 0, \tag{9}$$

where $\xi = v_R/v_t$ (v_R is the velocity of Rayleigh wave). (Graff, 1991) Solving Eq. (9), we obtain $\xi = 0.914$. A wave packet with z-polarized vector is used as an incident wave in order to excite SAWs in the system. Below the threshold frequency corresponding to the wavelength of SAWs equivalent to the periodicity of the array, both the transmission rates are coincident because the waves with long wavelength cannot recognize the geometrical difference. However, above the threshold frequency, the transmission rate shows obvious rectification of SAWs as well as periodic dips with respect to frequency, resulting from the strong interference effects of scattered SAWs. We also find the periodic structure of the transmission rate of case (II) is more pronounced than that of case (I) because the former makes the mode conversion more accessible than the latter due to the geometry of the scatterers.
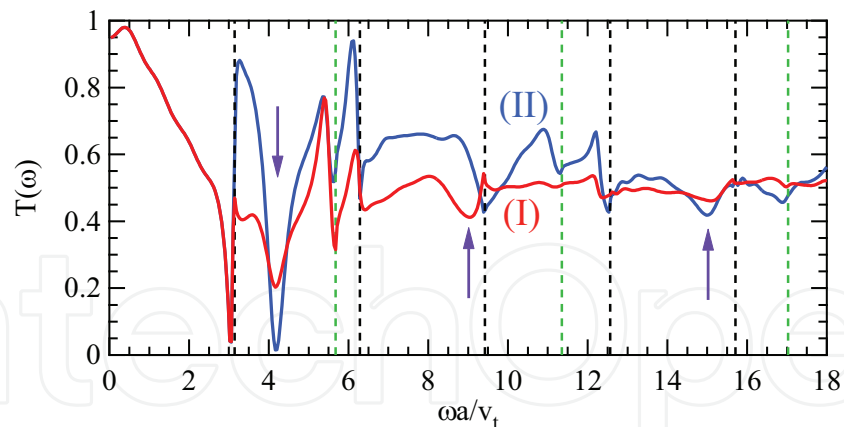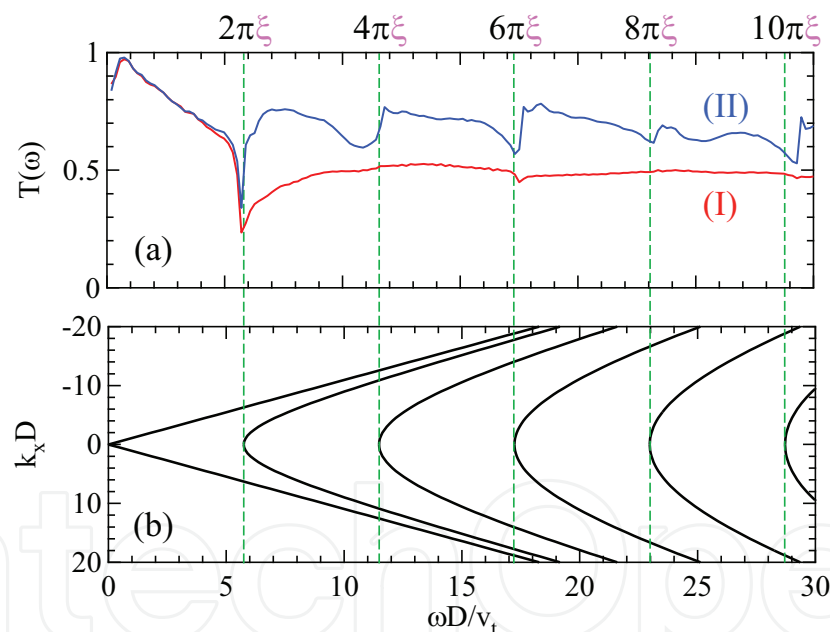
Fig. 5. Transmission rate versus frequency for mixed modes through single-array of triangular holes with $\alpha = \pi/3$. (I) and (II), designated by red and blue solid line, respectively, indicate the incident direction of acoustic waves. The vertical black dashed lines (as shown in Fig. 4) and green ones indicate the positions of $n\pi v_t/a$ and $n\pi v_l/a$, where v_l and v_t are the velocity of longitudinal and transverse waves, respectively, and n is a positive integer (n = 1, 2, 3, . . .). The arrows indicate the dips whose positions depend on the geometry of triangular holes such as the summit angle α and the length of base a.

Fig. 6. (a) Transmission rate versus frequency for SAWs through single-array of triangular holes with $\alpha = \pi/3$. The labels (I) and (II), designated by red and blue solid line, respectively, indicate the incident directions of SAWs. The vertical dashed lines indicate the positions of $2n\xi\pi v_t/D$, where n = 1, 2, . . . where $\xi = v_R/v_t$ (v_R and v_t are the velocity of Rayleigh and transverse waves, respectively). (b) Dispersion relation of SAWs within the framework of empty-lattice approximation.

Figure 6(b) shows the dispersion relation of SAWs within the framework of empty-lattice approximation to reveal the origin of the periodic dips in Fig. 6(a). Within the empty-lattice approximation the subband structures due to the periodicity of the y direction appear in the dispersion relation, which are given by

$$\frac{\omega D}{v_t} = \xi \sqrt{(k_x D)^2 + (2\pi n)^2}, \left(n = 0, \pm 1, \pm 2, \cdots\right).$$ (10)

The dispersion relation can be obtained by replacing the wavevector k in the dispersion relation of Rayleigh waves $\omega = v_R k$ by $\sqrt{k_x^2 + \left(k_y + 2\pi n / D\right)^2}$ where $2\pi n / D$ is the reciprocal lattice vector in the y direction. The dips in Fig. 6(a) correspond to the band edges of the subband structure, manifesting that the periodic dips in the transmission are due to the Bragg reflection of SAWs in the y direction. It should be noted that the shift of the band edges for the SAWs is modified by a factor of ξ as much as that for bulk transverse waves.

Figure 7 shows the efficiency for the rectification of SAWs which is denoted by black solid line. The thin blue lines indicate the efficiency for bulk transverse waves as reference. The efficiency for SAWs is lower than that for bulk waves because of the mode conversion from SAWs to bulk waves due to the triangular scatterers.

Figure 8 (a) shows the transmission rate versus frequency for shear horizontal (SH) modes through the single-array of triangular holes. For excitation of SH waves in the system, we use a wave packet with y-polarization vector as an incident wave. The threshold frequency above which the rectifying effect occurs becomes exactly $2\pi v_t / D$ where v_t is the velocity of SH waves. Above the threshold frequency, the transmission rates exhibit dips periodically at multiples of the threshold frequency due to the same mechanism as the SAWs and bulk waves. However, the SH waves are inefficient compared to the SAWs as shown in Fig. 8(b). The inversions between the transmissions of cases (I) and (II) occur around $\omega D / v_t \approx 18$.

4. Summary and future prospects

We proposed an acoustic-wave rectifier and numerically demonstrated the rectification effects on bulk waves as well as SAWs above the threshold frequencies. The rectification mechanism is due to the geometric effects of the asymmetric scatterers on acoustic wave scattering, which is enhanced by interference among the scattered waves. The threshold frequency for the rectification results from the periodic arrangement of scatterers. Hence, it is possible to tune the rectifier by adjusting the position of the scatterers. The findings of this work can be applied not only to sound waves in solids or liquids but also to optical waves, leading to new devices in wave engineering.
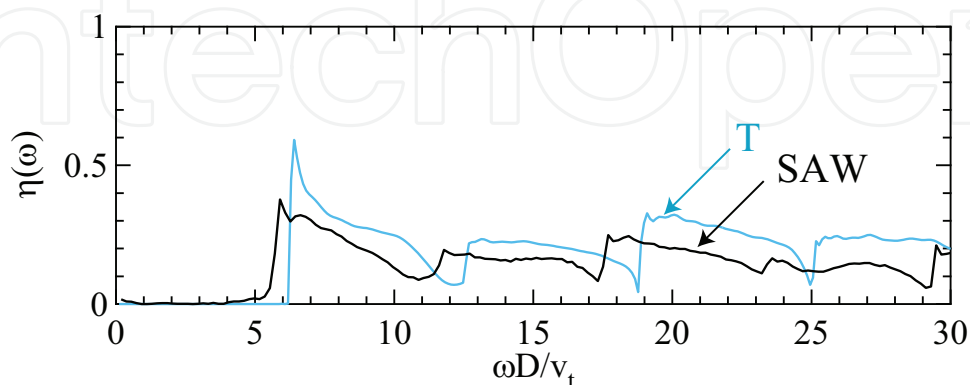

Fig. 7. Efficiency for the rectification of SAWs ($\alpha = \pi/3$). The solid black and thin blue lines indicate the efficiencies for SAWs and bulk single modes (T), respectively. The efficiency of the SAW rectifiers is slightly lower than that of the bulk single mode.
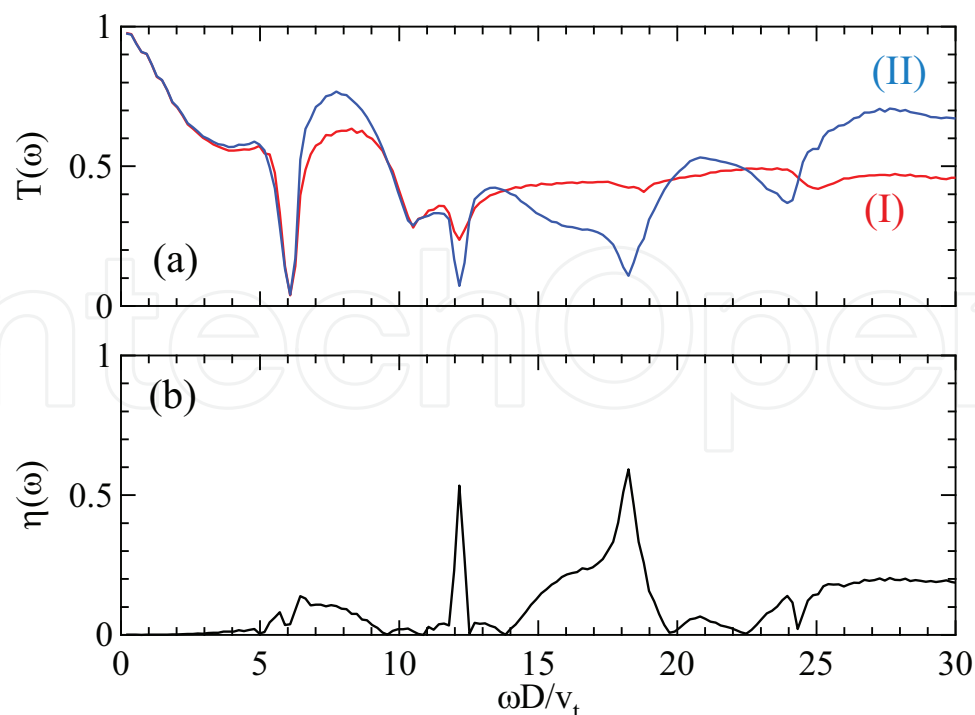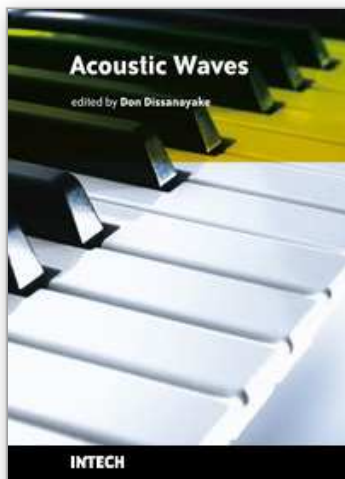
Fig. 8. (a) Transmission rate versus frequency for SH modes through single-array of triangular holes with $\alpha = \pi/3$. The labels, (I) and (II), designated by red and blue solid line, respectively, indicate the incident direction of acoustic waves. (b) Efficiency for the rectification of SH waves.

5. References

Chang, C.W., Okawa, D., Majumdar, A. & Zettl, A. (2006). Solid-state thermal rectifier, *Science* 314(5802): 1121–1124.

Fleischmann, R. & Geisel, T. (2002). Mesoscopic rectifiers based on ballistic transport, *Phys. Rev. Lett.* 89(1): 016804.

Graff, K. F. (1991). *Wave Motion in Elastic Solids*, Dover Publications.

Kittel, C. (2004). *Introduction to Solid State Physics, 8 edition*, Wiley.

Krishnan, R., Shirota, S., Tanaka, Y. & Nishiguchi, N. (2007). High-efficient acoustic wave rectifier, *Solid State Communications* 144(5-6): 194–197.

Liang, B., Yuan, B. & Cheng, J.-C. (2009). Acoustic diode: Rectification of acoustic energy flux in one-dimensional systems, *Phys. Rev. Lett.* 103(10): 104301.

Linke, H., Sheng, W., Löfgren, A., Xu, H.-G., Omling, P. & Lindelof, P. E. (1998). A quantum dot ratchet: Experiment and theory, *Europhys. Lett.* 44(3): 341.

Shirota, S., Krishnan, R., Tanaka, Y. & Nishiguchi, N. (2007). Rectifying acoustic waves, *Japanese Journal of Applied Physics* 46(42): L1025–L1027.

Song, A. M., Lorke, A., Kriele, A., Kotthaus, J. P., Wegscheider, W. & Bichler, M. (1998). Nonlinear electron transport in an asymmetric microjunction: A ballistic rectifier, *Phys. Rev. Lett.* 80(17): 3831–3834.

Tamura, S. (1985). Spontaneous decay rates of la phonons in quasi-isotropic solids, *Phys. Rev. B* 31(4): 2574–2577.

Tanaka, Y., Murai, T. & Nishiguchi, N. (n.d.). in preparation.

Acoustic Waves

Edited by Don Dissanayake

SAW devices are widely used in multitude of device concepts mainly in MEMS and communication electronics. As such, SAW based micro sensors, actuators and communication electronic devices are well known applications of SAW technology. For example, SAW based passive micro sensors are capable of measuring physical properties such as temperature, pressure, variation in chemical properties, and SAW based communication devices perform a range of signal processing functions, such as delay lines, filters, resonators, pulse compressors, and convolvers. In recent decades, SAW based low-powered actuators and microfluidic devices have significantly added a new dimension to SAW technology. This book consists of 20 exciting chapters composed by researchers and engineers active in the field of SAW technology, biomedical and other related engineering disciplines. The topics range from basic SAW theory, materials and phenomena to advanced applications such as sensors actuators, and communication systems. As such, in addition to theoretical analysis and numerical modelling such as Finite Element Modelling (FEM) and Finite Difference Methods (FDM) of SAW devices, SAW based actuators and micro motors, and SAW based micro sensors are some of the exciting applications presented in this book. This collection of up-to-date information and research outcomes on SAW technology will be of great interest, not only to all those working in SAW based technology, but also to many more who stand to benefit from an insight into the rich opportunities that this technology has to offer, especially to develop advanced, low-powered biomedical implants and passive communication devices.

How to reference

In order to correctly reference this scholarly work, feel free to copy and paste the following:

INTECH
open science | open minds